34th Annual International Conference of the IEEE EMBS
San Diego, California USA, 28 August - 1 September, 2012

Accelerated Phosphorus Magnetic Resonance Spectroscopic Imaging Using Compressed Sensing

Nurten C. Askin, Berna Atis, and Esin Ozturk-Isik

Abstract— **This study aims at assessing the performance of compressed sensing method for faster phosphorus magnetic resonance spectroscopic imaging (^{31}P-MRSI) of human brain. A simulated 2D ^{31}P-MRSI dataset containing a tumor region and a healthy region was created based on the metabolite peak intensities and ratios of a volunteer dataset acquired at 3T. k-space data was randomly undersampled, and reconstructed using compressed sensing algorithm. This simulation study showed that compressed sensing reconstruction could be applied for faster ^{31}P-MRSI. Future studies will measure the performance of compressed sensing reconstruction for ^{31}P-MRSI in volunteers and patients with brain tumors.**

I. INTRODUCTION

Magnetic resonance spectroscopic imaging (MRSI) is a magnetic resonance imaging (MRI) technique that could provide information about the biochemistry of the tissue. Phosphorus (^{31}P) MRSI can provide important information regarding the energetic and ischemic status, as well as membrane degradation and synthesis, and pH of the tissue. Phosphocreatine (PCr), phosphorylcholine (PC), phosphorylethanolamine (PE), inorganic phosphate (Pi), glycerophosphorylcholine (GPC), three different peaks for the ATP molecule, γ-ATP, α-ATP, and β-ATP peaks, and glycerophosphorylethanolamine (GPE) are the major metabolites observed with ^{31}P-MRSI.

The previous studies have reported phosphorus metabolite level differences in brain tumors and healthy brain tissue [1, 2]. When brain tissue gets ischemic, ATP production comes from hydrolysis of PCr catalyzed by creatine kinase leading to a reduction of PCr/β-ATP ratio in ^{31}P-MRSI [2], and the breakdown of glycogen to lactic acid which can be observed as the lactate peak in ^{1}H MR spectra [3]. Pi also increases at ischemia due to increased ATP hydrolysis that is not matched by ATP synthesis leading to a Pi/PCr increase [1]. Phosphorylcholine and phosphorylethanolamine are the phosphomonoesters (PME) that are produced from choline and ethanolamine phosphorylation during membrane synthesis. On the other hand, during membrane degradation, GPC and GPE are formed and these metabolites are collectively called phosphodiesters (PDE). Hubesch et al. reported a significant reduction in the PCr/Pi ratio, and an increase of pH levels in brain tumors [1]. Maintz et al. observed an alkaline environment (pH=7.16) and a decrease in the PCr and PDE peaks for meningiomas, and a slight alkalization (pH = 7.09) and more than a two fold reduction in the PDE/α-ATP ratio for low grade gliomas [2].

Although ^{31}P-MRSI provides non-invasive information about brain tumor biochemistry, it has not been widely acquired in clinical settings due to its long data scan time. Phosphorus is 15 times less MR sensitive than proton, and ^{31}P-MRSI requires larger voxels and averaging several acquisitions for adequate SNR. Obruchkov et al. has reported the implementation of flyback echo planar imaging (EPI) for acquiring faster ^{31}P-MRSI data [4]. However, flyback EPI pulse sequence is not routinely available in clinical settings and there might be data regridding errors in its reconstruction [5]. In another simulation study, Srinivasa-Raghavan et al. implemented generalized autocalibrating partially parallel acquisitions (GRAPPA) technique for the reconstruction of undersampled ^{31}P-MRSI data of the liver [6]. GRAPPA method can reconstruct undersampled data that is acquired using a multi-channel RF coil, but phosphorus sensitive multi-channel RF coils are not widely available in clinical settings. Additionally, signal to noise ratio (SNR) is proportional to the root of data acquisition time. So, an SNR loss would result while accelarating the ^{31}P-MRSI data acquisition with using either flyback EPI or GRAPPA methods. Compressed sensing is another fast data acquisition and reconstruction technique that can reconstruct randomly undersampled k-space data using a regularization algorithm such as conjugate gradient method. It has been proposed to accelerate MR data acquisition with less SNR penalty than other fast imaging techniques due to its denoising effect [7], and has been successfully applied for acquiring faster carbon (^{13}C) MRSI data [8, 9]. In this study, we have investigated the feasibility of applying compressed sensing method for accelerated ^{31}P MR spectroscopic imaging.

II. METHODS

A. Compressed Sensing

Compressed sensing is a recent technique that can provide an exact reconstruction of sparsely undersampled signals. It was first formulated by Dr. Emmanuel Candes while he was performing noise reduction experiments on a Shepp-Logan phantom, when l_1 norm reduction provided a perfect image

*Research supported by Marie Curie International Reintegration Grants (IRG) FP7-PEOPLE-RG-2009 256528.

N.C. Askin and B. Atis are with the Biomedical Engineering Department, Yeditepe University, Istanbul, 34755 TURKEY. (e-mail: ceren.askin@yeditepe.edu.tr, batis_53@hotmail.com).

E. Ozturk-Isik is with the Biomedical Engineering Department, Yeditepe University, Istanbul, 34755 TURKEY. (corresponding author, phone: (+90)216-578-0000; fax: (+90)216-578-0400; e-mail: esin.ozturk@yeditepe.edu.tr).

reconstruction [10]. For compressed sensing method to be applicable, three criteria need to be satisfied. First, the signal should be sparse in a transform domain, which means that it should have a few non-zero components in that domain. Second, the signal should be randomly undersampled, with a resultant incoherent aliasing pattern. Third, a nonlinear data reconstruction method like conjugate gradient method, that aims to find an approximate solution for an ill-posed problem should be utilized.

Lustig et al. implemented the first application of compressed sensing method for accelerated MR imaging [7]. In this first application, compressed sensing method was applied to acquire faster MR angiography and spin echo images. Hu et al. later implemented compressed sensing reconstruction of ^{13}C MR spectroscopic imaging [8, 9]. MR spectroscopic signals are naturally sparse, and they have few non-zero components along the spectral bandwidth at only certain frequencies and usually at a narrow linewidth. Furthermore, a sparse MR spectroscopic signal can be properly represented with a few large Wavelet components, which satisfies the first criterion of implementing compressed sensing method [8]. Compressed sensing reconstruction of randomly selected spectral data in (k, t) domain can be formulated as,

$$\begin{aligned} &\min\left(\left\|\psi(m)\right\|_1\right) \\ &s.t.\ \ \left\|F_a(m)-y\right\|_2 < \varepsilon \end{aligned} \tag{1}.$$

In equation (1), m indicates an approximate solution, $\Psi(m)$ is its Wavelet transform, $\|\ \|_1$ is the l_1 norm, F_a indicates a random undersampling operator in Fourier domain, y represents the original Fourier domain samples, and ε represents an error at noise level. The l_1 norm of the Wavelet transform of the approximate solution should be small, and the l_1 norm can be calculated as,

$$\left\|x(i)\right\|_1 = \sum_i |x(i)| \tag{2}.$$

According to (1), a correct solution's undersampled Fourier transform should be in good agreement with the original Fourier domain samples, and it should be sparse and compressible with Wavelet transform. These discrepancy and sparsity criteria can be transformed into a Lagrange form and written as an optimization problem as,

$$\min_m\left(\left\|F_a(m)-y\right\|_2 + \lambda\left\|\Psi(m)\right\|_1\right) \tag{3}.$$

Due to undersampling in Fourier domain, compressed sensing MRI reconstruction problem is an ill-posed problem with multiple solutions. Regularization methods are often employed for solving ill-posed problems. Conjugate gradient method is commonly used for the solution of the compressed sensing reconstruction problem [11].

B. Data Acquisition and Processing

One volunteer, who provided informed consent, was scanned on a 3T MR scanner (Philips Medical Systems, Best, Netherlands) using a surface ^{31}P coil. The coil had a disk at the center containing water and methylphosphonic acid, which was used as a localization reference. TFE survey images were acquired with the body coil (TR=75 ms, TE=5 ms, flip angle=30°). A ^{31}P MR spectrum was acquired from the frontoparietal lobe with image selected in vivo spectroscopy (ISIS) [12] (TR=5s, 128 averages, 3000 Hz, dwell time = 0.333 ms, 1024 points, 27cc voxel size, scan time=11 min). The spectrum was processed using apodization with a 10 Hz Gaussian filter, phase correction and baseline removal and quantified using AMARES [13] within jMRUI. The amplitude (a) and frequency (f) factors calculated for each peak, k, with AMARES were used to reconstruct the time domain signal in MATLAB (The Mathworks Inc., Natick, MA) for creating a spectrum of a healthy voxel as,

$$y_n = \sum_k a_k e^{-(d_k + i2\pi f_k)t_n} \tag{4},$$

where d_k was set to 30 Hz for all the peaks. Similarly, a spectrum of a tumor voxel was simulated. The peak amplitudes of the tumor spectrum were (0.49, 1.0, 1.0, 1.0, 2.16, 1.86, 1.47, 2.06, 2.63) times the peak amplitudes of the healthy spectrum for the PCr, γ-ATP, α-ATP, β-ATP, GPC, GPE, Pi, PC, and PE peaks, respectively. A 2D 32x32 ^{31}P MR spectroscopic imaging dataset that included a tumor region at the top left 10 by 10 voxels and a healthy region at the rest of the array was simulated using the healthy and tumor spectra.

A random undersampling pattern that reduced the k-space data along x by a factor of 2.23 was implemented in MATLAB. The central two lines of k-space were preserved due to SNR concerns [9]. The 2D sampling mask for one of the frequency points is shown in Figure 1. The reduced dataset was inverse Fourier transformed along k_y. For each y point, k_x-f data were reconstructed using the SparseMRI software package [7]. l_1-norm and total variation weights were chosen empirically as 0.01. A 1D length-4 Daubechies Wavelet transform was used as the sparsifying transform. Figure 2 shows the flowchart of data preparation.

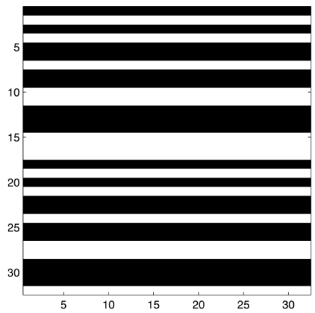

Figure 1. The random k-space undersampling pattern shown for one of the frequency points. In total, % 56.25 of all the k-space points were set to zero (R=2.23).

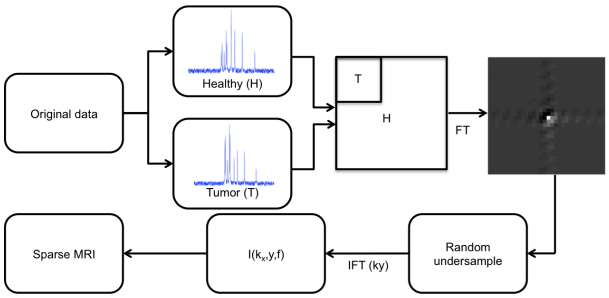

Figure 2. The flowchart of data preparation scheme.

A Bland Altman statistical test was utilized to detect if there was any significant differences between mean Pi/PCr, PCr/β−ATP, and PCr/PE ratios of the original and compressed sensing datasets within the tumor and healthy regions. For the Bland Altman method, the difference between all the pairs of a given peak ratio computed from the compressed sensing and original datasets was used. The mean difference, which is a measure of bias between the two observations, and the standard deviation of the difference were computed. The difference was plotted against the mean of the two observations for each point. If there were no outliers below or above two standard deviations of the mean difference, then two observations were thought to be in good agreement. A ranksum test was used to detect if the SNR of PCr, Pi and β−ATP were different between the tumor and healthy regions for the original and compressed sensing datasets. $p<0.05$ was considered as significant.

III. RESULTS

Figure 3 shows ^{31}P MR spectra of six voxels from the original and compressed sensing reconstructed datasets. The top three voxels had tumor spectra, and the other three voxels had healthy spectra. Tumor and healthy spectral regions were clearly separable in both spectral datasets. Tumor spectra had visibly lower PCr, and higher PME, PDE and Pi peaks. ATP peak levels were similar between the tumor and healthy regions.

Table 1 shows Pi/PCr, PCr/β-ATP, and PCr/PE metabolite ratios in tumor and healthy regions for the original and compressed sensing datasets. Tumor regions had higher Pi/PCr, and lower PCr/β-ATP and PCr/PE than the healthy regions for both datasets. Table 2 shows the results of the Bland Altman statistical test that looked at the bias and the variation of the peak ratios for the original and compressed sensing datasets. In healthy regions, metabolite ratios were similar between the original and compressed sensing datasets. The mean difference, or bias, in healthy regions was 0.01, 0.03, and 0.13 for Pi/PCr, PCr/β-ATP and PCr/PE ratios, respectively. In tumor regions, the bias was higher than the healthy regions. There were no outliers in the tumor region, showing that the variation of the differences between the peak ratios was low in that region. There were around 20 outliers in the healthy region for each peak ratio.

Table 3 shows the signal to noise ratio (SNR) of PCr, Pi, and β-ATP peaks in tumor and healthy regions and the SNR ratio between these two regions for the original and compressed sensing datasets. The denoising effect of compressed sensing reconstruction resulted in higher SNR for all the peaks. Tumor regions had a higher denoising than healthy regions resulting in higher tumor/healthy SNR ratios than the original dataset. According to the results of a ranksum test, SNR of PCr was statistically significantly lower ($p<0.001$), and SNR of Pi was significantly higher ($p<0.001$) in tumor regions than healthy regions for both the original and compressed sensing datasets. Although β-ATP SNR levels were very similar in tumor and healthy regions, there was a statistically significant difference between them ($p<0.001$) due to the higher number of voxels considered.

Table 4 shows the tumor over healthy mean peak height ratios of PCr, Pi and β-ATP for the original and compressed sensing datasets. The tumor spectrum was simulated to have 0.49, 1.0, and 1.47 times the peak amplitudes of the healthy spectrum for the PCr, β-ATP, and Pi peaks, respectively. Compressed sensing and original datasets both had similar ratio of tumor over healthy mean peak heights.

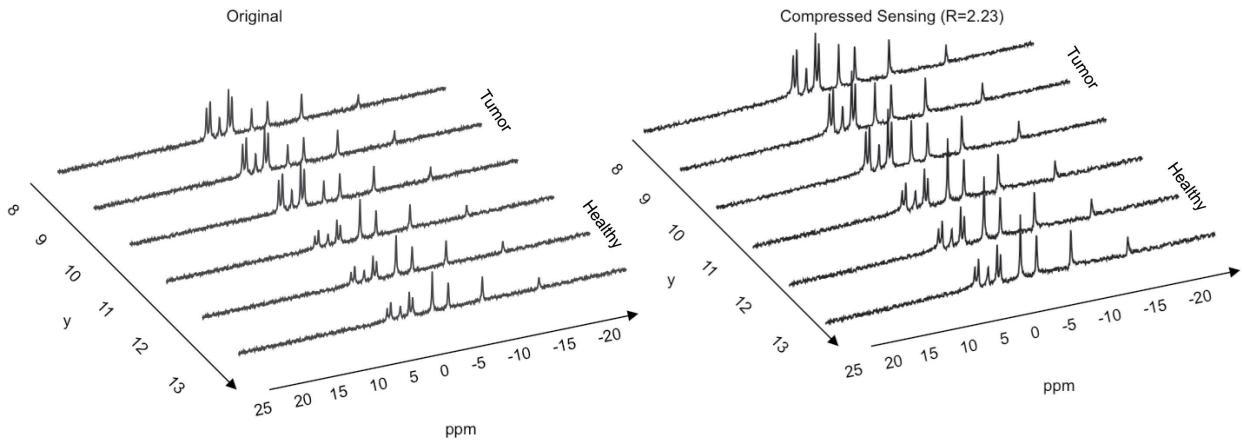

Figure 3. Six voxels showing the transition between the healthy and tumor voxels for the original and compressed sensing reconstructed datasets.

TABLE I. PI/PCR, PCR/β−ATP, PCR/PE METABOLITE RATIOS IN TUMOR AND HEALTHY REGIONS OF THE ORIGINAL (O) AND COMPRESSED SENSING (CS) DATASETS.

Metabolite Ratios (mean±std)		***Pi/PCr***	***PCr/β-ATP***	***PCr/PE***
CS	Tumor	0.80±0.03	2.04±0.07	0.77±0.04
	Healthy	0.34±2.4e-05	3.09±4.2e-04	2.68±3.4e-04
O	Tumor	1.05±0	1.70±0	0.56±0
	Healthy	0.35±0	3.06±0	2.80±0

TABLE II. BLAND ALTMAN TEST STATISTIC RESULTS FOR THE DIFFERENCE BETWEEN THE PEAK RATIOS OF THE ORIGINAL AND COMPRESSED SENSING DATASETS IN TUMOR AND HEALTHY REGIONS.

Bland Altman Test Results		***Pi/PCr***	***PCr/β-ATP***	***PCr/PE***
Tumor	# outliers	0	0	0
	mean(difference)	0.25	0.34	0.21
	std(difference)	0.03	0.07	0.04
Healthy	# outliers	20	27	20
	mean(difference)	0.01	0.03	0.13
	std(difference)	2.45e-5	4.16e-4	3.53e-4

TABLE III. SNR VALUES OF PCR AND PI PEAKS IN TUMOR AND HEALTHY REGIONS AND THEIR RATIOS OF THE ORIGINAL (O) AND COMPRESSED SENSING (CS) DATASETS.

SNR (mean±std)		***Tumor***	***Healthy***	***Tumor/Healthy***
CS	PCr	46.13±3.11	57.53±0.06	0.80
	Pi	37.03±1.76	19.46±0.02	1.90
	β−ATP	22.59±1.21	18.60±0.02	1.21
O	PCr	19.73±0	42.68±0	0.46
	Pi	20.77±0	14.77±0	1.41
	β−ATP	11.62±0	13.95±0	0.83

TABLE IV. THE RATIO OF MEAN PEAK HEIGHTS OF PCR, PI, AND β-ATP WITHIN HEALTHY AND TUMOR REGIONS OF THE ORIGINAL AND COMPRESSED SENSING DATASETS.

Ratio of Tumor/Healthy Mean Peak Heights	***PCr***	***Pi***	***β-ATP***
Compressed Sensing	0.59	1.40	0.89
Original	0.52	1.59	0.94

IV. CONCLUSION

This study investigated the feasibility of using compressed sensing method for reducing the scan time of ^{31}P MR spectroscopic imaging. Our results showed that compressed sensing reconstructed data had higher SNR than the original data due to the denoising effect. But, peak height ratios were similar between the original and compressed sensing datasets. The implementation of the compressed sensing technique could be further improved by acquiring fewer k-space lines. Future studies will measure the performance of compressed sensing reconstruction for ^{31}P-MRSI in volunteers and patients with brain tumors.

REFERENCES

[1] Hubesch, B., et al., *P-31 MR spectroscopy of normal human brain and brain tumors.* Radiology, 1990. **174**(2): p. 401-9.

[2] Maintz, D., et al., *Phosphorus-31 MR spectroscopy of normal adult human brain and brain tumours.* NMR Biomed, 2002. **15**(1): p. 18-27.

[3] Alger, J.R., et al., *Metabolism of human gliomas: assessment with H-1 MR spectroscopy and F-18 fluorodeoxyglucose PET.* Radiology, 1990. **177**(3): p. 633-41.

[4] Obruchkov, S., *Echo Planar Spectroscopic Imaging and 31P In Vivo Spectroscopy. Open Access Distertations and Theses. Paper 4121.*, 2011, McMaster University.

[5] Zierhut, M.L., et al., *(1)H spectroscopic imaging of human brain at 3 Tesla: comparison of fast three-dimensional magnetic resonance spectroscopic imaging techniques.* J Magn Reson Imaging, 2009. **30**(3): p. 473-80.

[6] Srinivasa-Raghavan, R., et al. *31P Spectroscopic Imaging with GRAPPA*. in *Conference Proceedings of 17th International Society of Magnetic Resonance in Medicine*. 2009. Hawaii, USA.

[7] Lustig, M., D. Donoho, and J. Pauly, *Sparse MRI: The application of compressed sensing for rapid MR imaging.* Magnetic resonance in medicine, 2007. **58**(6): p. 1182-1195.

[8] Hu, S., et al., *Compressed sensing for resolution enhancement of hyperpolarized 13C flyback 3D-MRSI.* J Magn Reson, 2008. **192**(2): p. 258-64.

[9] Hu, S., et al., *3D compressed sensing for highly accelerated hyperpolarized (13)C MRSI with in vivo applications to transgenic mouse models of cancer.* Magn Reson Med. **63**(2): p. 312-21.

[10] Candes, E.J. and J. Romberg. *Practical signal recovery from random projections*. in *Proc. SPIE Computational Imaging*. 2005. San Jose.

[11] Shewchuk, J. *An introduction to the conjugate gradient method without the agonizing pain*. 1994.

[12] Ordidge, R., A. Connelly, and J.A. Lohman, *Image-selected in vivo spectroscopy (ISIS): A new technique for spatially selective NMR spectroscopy.* J Magn Reson, 1986. **66**: p. 283-294.

[13] Vanhamme, L., et al., *Time-domain quantification of series of biomedical magnetic resonance spectroscopy signals.* J Magn Reson, 1999. **140**(1): p. 120-30.